Applied Physics A (2022) 128:861
https://doi.org/10.1007/s00339-022-06002-0

Applied Physics A
Materials Science & Processing

Effect of doping with manganese and zinc on the structural, morphological, optical and photocatalytic properties of NiO

Nahla Djebbari[1,2] · Dikra Bouras[2] · Hichem Farh[2,3]

Received: 13 June 2022 / Accepted: 24 August 2022
© The Author(s), under exclusive licence to Springer-Verlag GmbH, DE part of Springer Nature 2022

Abstract
A compound that has not been used before represented in powders consisting mainly of nickel oxide doped with 15%, 25% and 50% zinc and manganese which was prepared from expired materials. To obtain these samples, Sol–gel method was use. These powders were studied to identify their structural properties using X-ray rays (XRD) while the scanning electron microscope (SEM) showed a spherical shape after addition. The results of infrared (IR) tests also showed the emergence of the chemical bonds Ni–O, Mn–O and Zn–O appearing in the frequency range [400–750]cm^{-1}.The optical properties showed a noticeable increase in the optical absorbance when doping with Mn and Zn, especially in the visible region. On the other hand, we were able to identify the extent of its effectiveness in the photocatalytic process by measuring the rate of decomposition, as we obtained a total purification of all dyes in the orange II polluted solution using the compound 25% MZNO within a period of time that did not exceed 25 min.

Keywords Expired nickel chloride · MZNO nanopowder · Sol–gel · Photocatalytic

1 Introduction

Lack of powders and their expiration date is one of the most common problems that face researchers while performing experiments. From here the idea of this research came, instead of throwing the powders away, researchers find that these materials can be used in applications that benefit society and the environment. Nowadays, photocatalysis considered among the most promising application which is an advanced technology that converts solar energy into sustainable fuels and oxidizes pollutants by aiding semiconductor photocatalysts [1–3]. The main scientific and technological challenges for efficient photocatalysis are the stability, robustness and efficiency of semiconductor photocatalysts. For practical applications, researchers are trying to develop highly efficient and stable photocatalysts [4, 5].

Over the past few decades, nanomaterials have attracted great interest due to their quantum size effects that exhibit unique magnetic, optical, electrical and catalytic properties. The unique chemical and physical properties of these engineered transition metal oxide particles are demonstrated compared to their bulk counterparts and are used in a multitude of chemical, physical, biomedical, biological and pharmaceutical applications [6]. Nanotechnology has also boosted ancient fields of knowledge due to the simple reduction in the size of the crystals. New forms were created, which led to the increase in performance or changes in the chemical properties of the materials [7].

Nickel oxide (NiO) is a p-type semiconductor and binary material characterized by a wide band gap located between (3.6–4.0 eV) [7, 8], known for these dielectric properties with selectivity in the optoelectronic field [5]. This semiconductor has better stability and lower knockout compared to other semiconductors such as ZnO and GaN [6]. It presents a promising candidate for multi applications depending on the methods of preparing it either in powder or in thin layers, including the super capacitor [8], the electrical device [9, 10], photocatalysis [11], and the gas sensor [5, 12]. Because of these properties, many processes have been proposed to produce this semiconductor (thin layer or nanoparticles) by different means, whether physical or chemical [13]. Nickel

✉ Hichem Farh
farhichem@gmail.com

[1] University Larbi Tebessi, 01200 Tebessa, Algeria

[2] Laboratory of Active Components and Materials (LCAM), University of Oum El Bouaghi, 04000, Oum El Bouaghi, Algeria

[3] University of Oum El Bouaghi, 04000, Oum El Bouaghi, Algeria

Published online: 05 September 2022

oxides are typically synthesized by a variety of methods including solid-state reaction, co-precipitation, spray drying, cryogenic (freeze drying) chemistry and gelation (particularly using amorphous compounds of citrate) [14]. To obtain a high-quality surface with good chemical homogeneity, the sol–gel method for the fabrication of NiO nanoparticles was successfully selected [15].

The search for new materials in the field of catalysis applied on industrial processes is an important economic issue. This research is specifically directed towards the preparation of high-performance catalysts which must meet certain criteria which are long-term chemical and mechanical stability, high catalytic activity, ease of implementation and low cost. However, it is difficult to combine all these requirements in one material, especially since it is in the state of expiration. As a result, two elements with high catalytic properties were added, manganese oxide and zinc, which have an energy gap less than nickel oxide 1.42 eV and 3.4 eV, respectively [16].

Manganese oxides MnO_2 have attracted a great deal of interest for organic dye contaminant removal due to their unique compositions and physical and chemical properties present in a wide range of polymorphs [17, 18]. Whereas, the removal efficiency of dye contaminants depends not only on their crystal forms and how they are formed but also on particle size, crystallization method and bulk density [19, 20]. Its use as a powder gives a high-quality surface useful for the photocatalytic process [19–21].

Suspended in water, zinc oxide can act as a photochemical catalyst for a number of reactions such as the oxidation of oxygen to ozone, the oxidation of ammonia to nitrate, the reduction of methylene blue and orange II, the synthesis of hydrogen peroxide, or the oxidation of phenols. More recent work studies new shapings of ZnO for applications as catalysts or sensors with good chemical properties [22].

In this work, we produced a compound of MZNO nanostructured powders based on nickel chloride material that expired in 2016. For the first time, the structural and optical properties of this compound were studied, and it was used for photocatalysis that was applied to a solution with orange II dye in the presence of visible light which we were able to completely get rid of toxic impurities present in the solution.

2 Experimental procedure

2.1 Characterization techniques

By X-ray diffraction (Bruker AXS-D8) the crystal structure of the powder particles was determined using Cu Kα radiation ($\lambda = 1.5406$ Å). To investigate the grain shape and size, a scanning electron microscope (JSM-6301F) and the infrared spectroscopy (Bruker II-RAM) was used to distinguish between the various chemical bonds of the prepared powders. The absorption spectra of the OII solutions were measured by a UV-vis spectrophotometer (V-630, JASCO) in the wavelength range [200–900 nm].

2.2 Materials

To prepare the powders, many materials were used namely, Expired Nickel II Chloride hexhydrate (Year2016), ($NiCl_2.6H_2O$), absolute ethanol (C_2H_5OH), Zinc Acetate ($(CH_3COO)_2$, $Zn.2H_2O$), Manganese II Acetate ($Mn(CH_3CO_2)0.2H_2O$), Monoethanolamine (C_2H_7NO) (MEA), Orange II($C_{16}H_{11}N_2NaO_4S$).

2.3 Preparation of nano-powders by Sol–gel method

2.3.1 NiO nano-powders

In becher, we put 30 ml of pure ethanol, add to it a mass of 6 g of nickel chloride and 2 ml of MEA. Then, the mixture is placed on a magnetic stirrer for an hour at an estimated temperature of 70 °C. After that, the solution is placed in a heat treatment oven at 500 °C during two hours. Thus, we get green nickel oxide powder (Fig. 1).

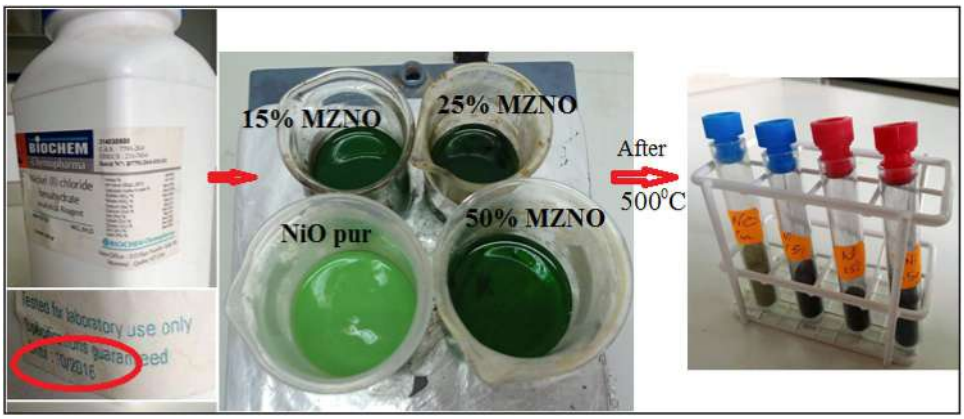

Fig. 1 Method of preparing powders from expired nickel

2.3.2 Mn–Zn co-doped NiO nano-powders

With the same weight as the previous experimental protocol, we add 15%, 25% and 50% to the nickel in the case of grafting it with manganese and zinc together. Thus, we get three black powders (Fig. 1): 15% MZNO, 25% MZNO and 50% MZNO (Mn–Zn co-doped NiO).

3 Characterization techniques

3.1 Measurement of photocatalytic activity

The photocatalytic activity of the various samples was measured by monitoring the absorption evolution of a solution containing OII (13 mg/L) colored dye. 0.2 g of nickel oxide powders with or without doping (Mn–Zn) is immersed in 25 ml of the dye solution. To speed up the reaction, the four samples were placed after closing them well over a magnetic stirrer (500 r/m) under visible light (Fig. 2). After every 5 min, 4 ml of the solution is withdrawn and placed in a sealable tube. The latter is subjected to a centrifugal force at 3500 units/min during 5 min to remove the catalyst. The solution was analyzed by UV-Vis absorption spectra measurements [300–650] nm using distilled water as a reference. The decomposition absorption rate is calculated from the maximum absorption spectra using the following equation [22, 23]:

$$D\% = \frac{C_0 - C}{C_0} \times 100 \quad (1)$$

where C_0 and C are the initial concentration before and after illumination, respectively.

4 Results and discussion

4.1 X-ray Diffraction

Figure 3a, b shows the X-ray diffraction curves of all the prepared films, and through the analysis of these curves, the locations of the peaks that appear sharply when beams of these rays are shined at different angles on the membrane were known to allow them to overlap constructively when the Bragg condition is available. We note that the three dominant trends of nickel powder growth are (200), (111) and (220) (JCPDS 04-0835) and there is no change in the prevailing trend with an increase in the percentage of grafting with manganese and zinc (Fig. 3a). The diagnostic results showed that it has a polycrystalline structure of cubic type. After doping with manganese and zinc, we notice the emergence of peaks corresponding to the crystal plans (100), (002), (101), (102), (110), (103) and (112) of the polycrystalline ZnO with a hexagonal structure of the type of Wurtzite. The diffraction peaks with plans (101), (111), (211) and (220) can be traced back to MnO_2.

The effect of doping inside the crystal structure has a major role in changing most of the physical properties, as the added doping atoms change the size of the crystal and thus the distance between the crystal levels, which in turn causes the positions of the peaks in the diffraction angle 2Θ axis to shift towards larger values (Fig. 2b).This is due to the placement of Mn^{2+} ions (0.67 Å), which is less than the size of Ni^{2+} ions (0.69 Å) in filling the interatomic gaps between the atoms in the lattice. This reduces some of the (smaller) Ni^{3+} ions to the Ni^{2+} oxidation state and thus, the lattice expands and the electronic conductivity of the material also decreases. On the other hand, the added Zn^{2+} ions (0.74 Å) cause interesting physical changes in the nickel lattice, increasing the crystal size due to the deformation.

Table 1 confirms this, as a larger particle size was obtained after doping with zinc and manganese, the grain size D is calculated by applying the Debye–Scherrer formula [23]:

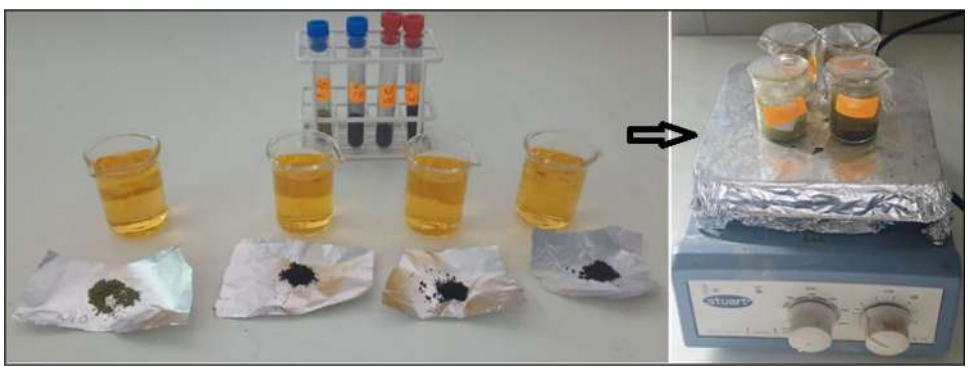

Fig. 2 Photocatalytic process

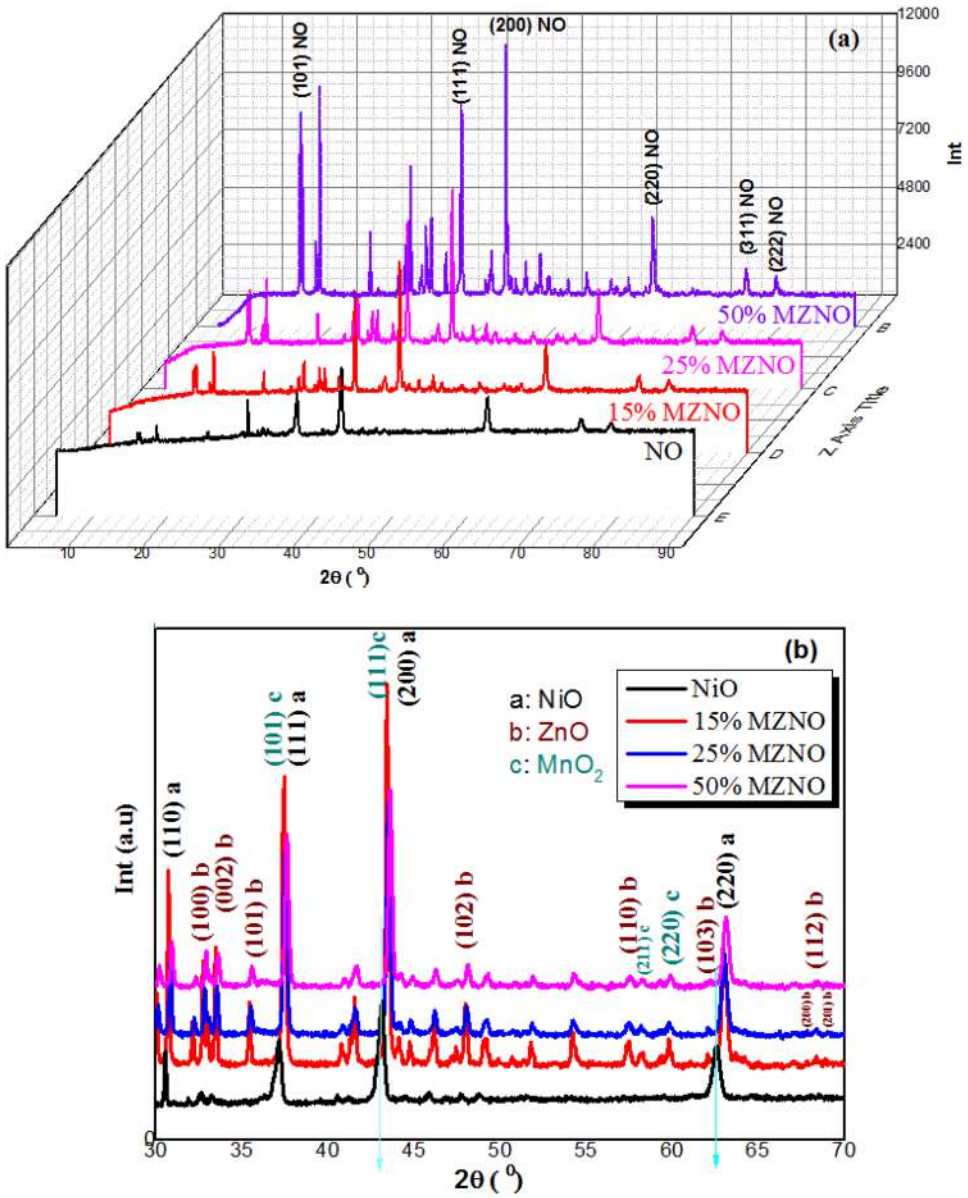

Fig. 3 XRD of NiO nanoparticles prepared from expired material and doped with different Zn/Mn ratios

Table 1 The grain size of the samples prepared before and after doping

Phases	Plan (hkl)	2Θ(°)	Θ(°)	FHWM β(°)	β (rad)	D (nm)
NiO	(111)	37.14	18.57	0.347	0.00605692	24.14
	(200)	43.13	21.565	0.448	0.007819075	19.05
	(220)	62.58	31.29	0.45	0.007853981	20.65
15% MZNO	(111)	37.46	18.73	0.23	0.004014257	36.45
	(200)	43.41	21.705	0.24	0.00418879	35.61
	(220)	62.97	31.485	0.34	0.005934110	27.39
25% MZNO	(111)	37.51	18.755	0.26	0.004537856	32.25
	(200)	43.50	21.75	0.26	0.004537856	32.88
	(220)	63.01	31.505	0.36	0.006283185	25.87
50% MZNO	(111)	37.61	18.805	0.25	0.004363323	33.55
	(200)	43.61	21.805	0.26	0.004537856	32.9
	(220)	63.11	31.555	0.38	0.006632251	24.52

$$D = \frac{K\lambda}{\beta cos\theta} \quad (2)$$

where: λ is the wavelength, βFWHM (full width at half maximum) and θ is the position of the diffraction peak considered.

4.2 Scanning Electron Microscopy (SEM)

To confirm the results obtained previously by XRD (3.1), we carried out morphological analyzes by scanning electron microscopy (SEM). Figure 4 displays the SEM images of NiO undoped, 15% MZNiO and 25% MZNiO. These images confirm the morphology differences between the three types of nanopowders. The grains of the substrates containing Mn and Zn are larger with a rounded shape and appear clearly after addition (Fig. 4b, c). Unlike this, for nickel oxide the grains are smaller, compact and adjacent to each other (Fig. 4a).

After depositing, the difference between the surfaces is more pronounced. The nanopowder (Mn, Zn) co-doped NiO the spherical-like growth dominates (Fig. 4c), it is the ideal and preferred form of photocatalysis as it provides a wider active surface area.

4.3 IR spectra

To study the properties of the chemical bonds of the prepared samples and to determine the locations and types of the apparent vibrational bonds, infrared spectroscopy was used by scanning wavelengths [400–4000]. Figure 5 shows the appearance of the absorption peak of the Ni–O bond in the transmittance curve of the pure powder at frequency 423.57 $cm^{-1}$and 555.74 cm^{-1}[24]. The absorption bands in the field 2361 cm^{-1} and 3388 cm^{-1} characterize the vibration of O-C-O and O–H bonds of carbon dioxide and water molecules, respectively [24]. The bands are observed at 1123.88 cm^{-1} and 1600 cm^{-1} assigned to the C–H vibration of the organic residues [25].

After doping with manganese and zinc (15%, 25% and 50%), we notice the appearance of changes in the pure absorption spectrum gradually in the range between 650 and 1500 cm^{-1}. The process of adding oxides led to a decrease in the intensity of the nickel oxide spectrum in the range [400–750] cm^{-1} to form the absorption peaks at 407 cm^{-1}

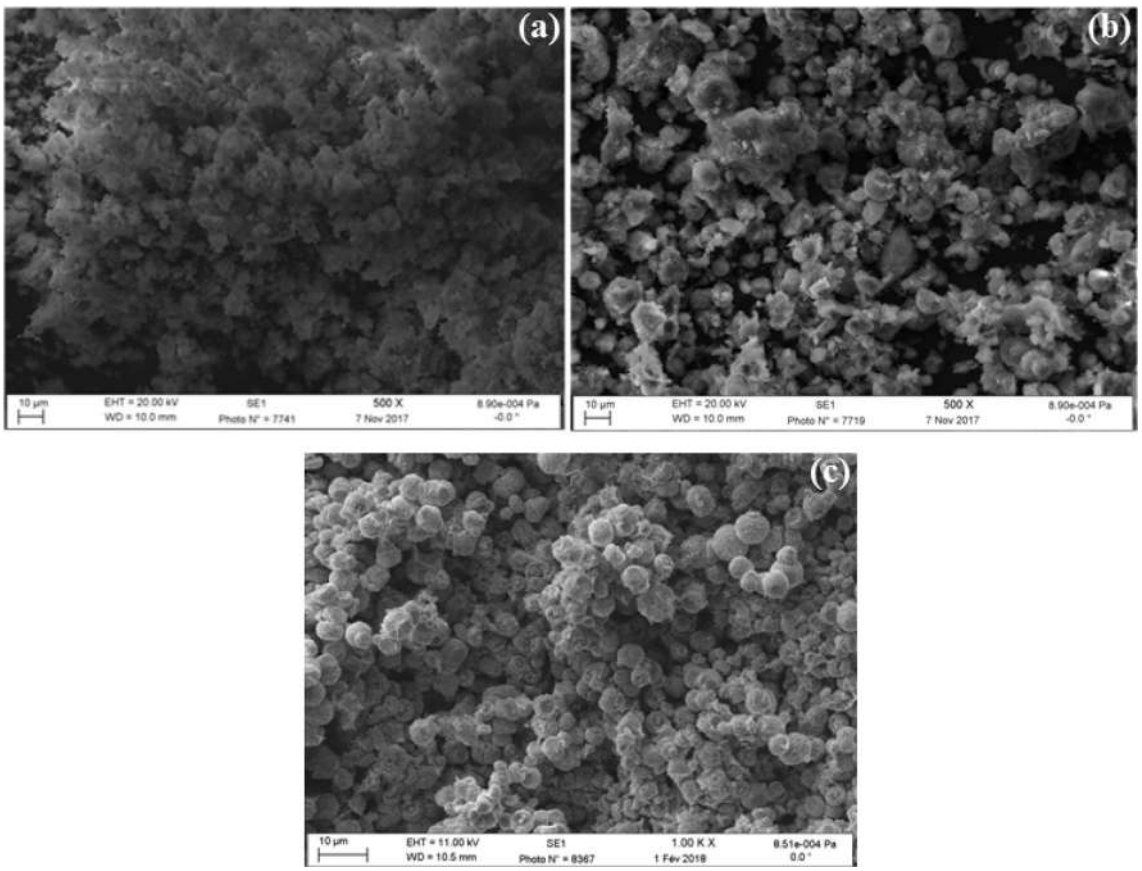

Fig. 4 SEM images of NiO (**a**), 25.wt % (Mn, Zn) co-doped NiO **b** and 25.wt % (Mn, Zn) co-doped NiO (**c**)

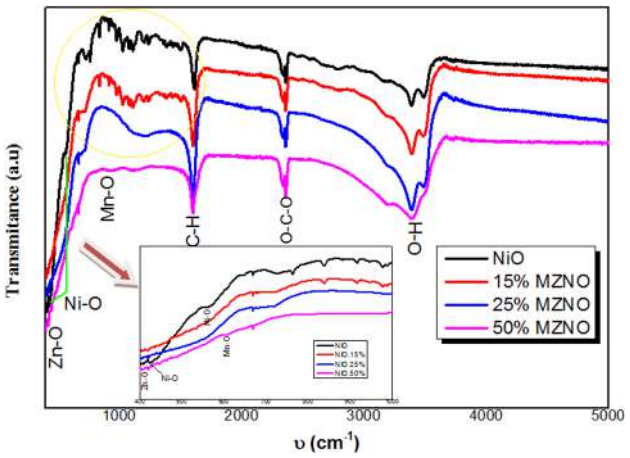

Fig. 5 Infrared spectrum of samples prepared and treated at 500 °C

and 401 cm^{-1} following the Zn–O bond vibration [26] and 731 cm^{-1},604.51 cm^{-1} following Mn–O bond vibration [27]. The presence of noise for the powders NiO and 15%MZNO in the range [650–1500] cm^{-1} could be due to the high moisture content present in the expired nickel chloride powder in which the powders were prepared, while it disappears when the percentage of doping by 25% and 50% for the two samples is 25%MZNO and 50%MZNO, respectively.

4.4 Optical analysis

The absorbance measurements were studied within the wavelength range (200–900 nm) for all the prepared nickel oxide powders dotted with manganese and zinc in four different ratios (0%, 15%, 25% and 50%). The absorbance relationship was plotted as a function of the wavelength as shown in Fig. 6, and the results showed that the absorbance increases with increasing wavelength for all doped powders (except for pure nickel oxide). Its values show that they are the lowest possible in the ultraviolet wavelengths region of the spectrum within the range 200–400 nm, and the absorbance values begin to gradually increase with the increase in wavelength values in the visible region 400–700 nm, then we notice that their values are almost stable in the infrared region. Nickel oxide has a very weak absorbance, but it quickly increases at the rate of doping, due to the presence of an increase in the absorption of visible light energy, which corresponds to an increase in the number of electronic transitions between the transmission band and the valence band, as the light energy is greater than the absorption edge. Also, there are levels of impurities (Mn and Zn) inside the energy separator that lead to an increase in the absorbance and thus a decrease in the permeability. The increase in the photocatalytic effect is mainly attributed to the increase in the reaction surface. However, the absorbance slightly decreases at the high percentage of 50% doping, and this was confirmed by the results of photocatalysis.

4.5 Optical gap

Gap value was calculated using Tauc's equation and the corresponding Tauc's plot which is shown in Fig. 7. The samples prepared used the following relation [26]:

$$\alpha h\nu = A \bullet \left(h\nu - E_g\right)^{1/2}. \quad (3)$$

with A: Constant, Eg: Optical Gap, $h\nu$: The energy of a photon.

The plot gives a straight line in a photon energy range, suggesting that the nanopowders has a direct electronic transition with a band gap of 2.48 eV, 2.62 eV and 2.80 eV for 15% MZNO, 25% MZNO and 50% MZNO, respectively. This transition comes from the crystal field splitting of the

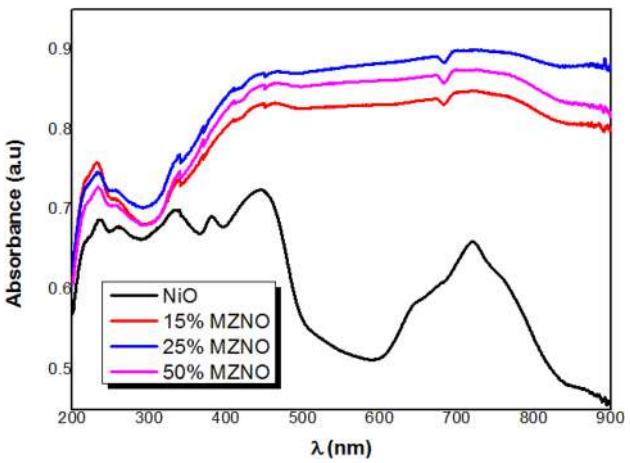

Fig. 6 UV–Vis Absorption Spectra of the catalysts

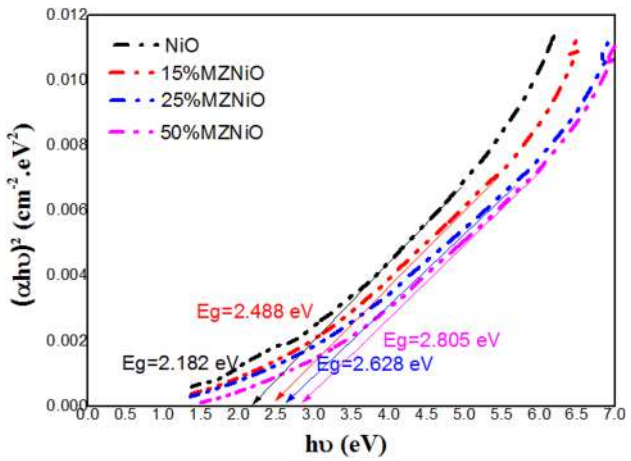

Fig. 7 Tauc plot of NiO, 15%MZNO, 25%MZNO and 50%MZNO nanopowders for determining the band gap

Mn^{4+} incomplete shell ($3d^3$), in conformity with the black color of γ-MnO_2 [27, 28]. This indicates that MZNO compound can absorb wavelengths in the visible range. Therefore, it can be proposed as photocatalyst under the visible light.

4.6 Photocatalytic performance

To determine the effectiveness of the new compound MZNO prepared with Sol–gel technology on the decomposition of the organic dye Orange II, the absorbance of the solutions was measured in the range of 300–650 nm. The obtained absorbance spectra are revealed in Fig. 8. MZNO powders were prepared with additives in different proportions, 15%, 25% and 50% by weight. In the case of NiO, during the process of photocatalysis, the color of the solution changed from orange to green, and two spectra of the OII dye appeared at a maximum wavelength of 484 nm and the other of the molecules of the added compound at a maximum wavelength of 393 nm (Fig. 8a). This phenomenon began to disappear with the addition of percentages 25% and 50% by weight of (Mn–Zn) (Fig. 8c, d), where the percentage of

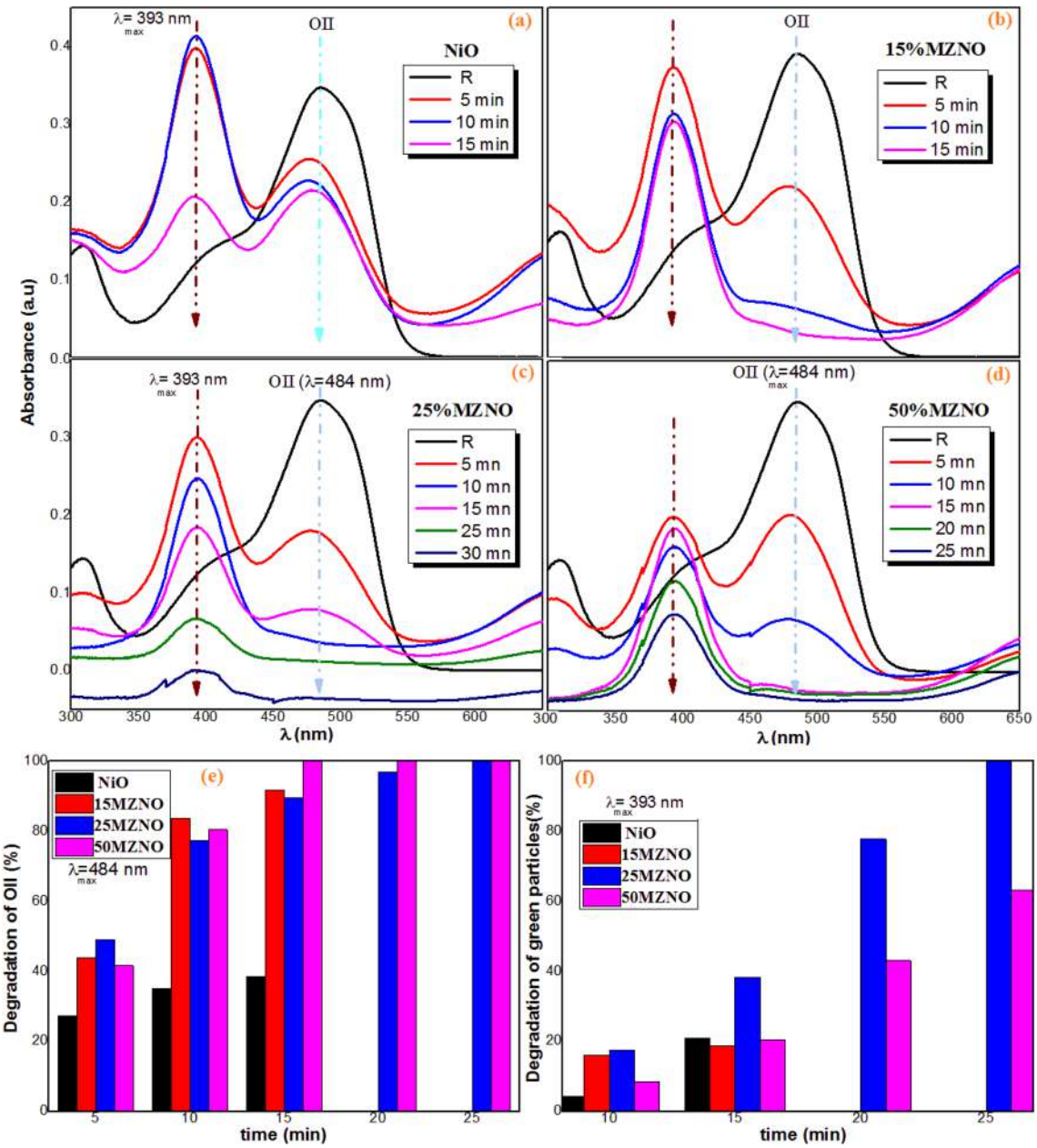

Fig. 8 Degradation rate of Orange II versus UV exposure time for **a** NiO, **b** 15% Mn–Zn co-doped NiO, **c** 15% Mn–Zn co-doped NiO and **d** 15% Mn–Zn co-doped NiO

decomposition of the dye spectrum reached 96.92% within 20 min for percentage 25%, while it reached 100% within 15 min (Fig. 8e). While there was a gradual decrease in the second spectrum, λ = 393 nm, the total decomposition rate was estimated (100%) within a time of 25 min for the 25% ratio of addition (25MZNO), during which we obtained a white solution; on the other hand, the decomposition rate was 63.16" for the addition of 50% (50MZNO) during the same time period (Fig. 8f). It can be said that the dopant ratio of the new compound 25MZNO has greater activity during photocatalysis (Fig. 8c).

Compared to previous work, working with expired materials is a new idea that has not been used before by researchers. Where the latter enabled us to obtain a very positive and motivating result to work with, and even gave a result similar or better than its predecessors. Fatsah Moulai et al. used γ-MnO_2 on his own and came up with what we found in 270 min [27], while the photolysis study by Naseer Ahmad Khan et al. showed that NiO NPs and NiO/Nc NC degraded about 93% and 96% orange II in aqueous medium, respectively, within 20 min [29].The MnO_2/NiO nanocomposite was selected by Xinyu Zhang et al. for the decomposition of orange II as it showed the best dye removal efficiency of 92.8% of NiO(67.80%) [30]. Therefore, the studied MZNO nanocomposite leads to a reduction in recombination and an increase in optical activity in the visible field, making it more competitive in practical industrial applications than other heterogeneous catalysts.

4.7 Photocatalytic mechanism

The photolysis of OII in aqueous solution using semiconductor nanoparticles can be explained by the mechanism of adsorption, oxidation and desorption [13, 14, 27, 28]. The energy gap of the three oxides, NiO, ZnO and MnO_2, estimated at 2.18 eV, 3.4 eV and 1.42 eV, respectively, enables them to generate electron/hole pairs (e^-/h^+) during their absorption of light energy (Eq. 5). The doping of nickel oxide with manganese and zinc led to a reduction in recombination and an increase in optical activity in the visible field. The optical excitation of MZNO nanoparticles led to the transfer of electrons from the valence band to the conduction band leaving behind holes, which is called oxidation–reduction reactions. From the electrons in the conduction band that interact with molecular oxygen to produce superoxide radical ions ($\bullet O_2^-$) and hydroperoxyl radicals ($\bullet HO_2^-$) (Eq. 7), while the holes in the valence band are confined to the space of hydroxyl ions to create the roots OH• (Eq. 8).Creating a greater number of OH• and $\bullet HO_2^-$ radicals led to high oxidation, which are the factors that contributed to attacking and disintegrating organic dye molecules (Eq. 9). The separation and migration mechanism of photo-generated electron–hole pairs of the MZNO compound through a schematic illustration (Fig. 9).

In this case, electrons of NiO and ZnO can reduce O2 to $\bullet O_2^-$. However, this reaction is impossible for MnO_2, because of its positive CB edge potential (− 0.01 eV) [27]. Thus, the process begins when the holes interact with water to produce hydroxide, and the electrons react with oxygen to induce a transparent color of the contaminated solution. The $\bullet O_2^-$ may then react with H_2O to form $HO_2\bullet$ and H_2O_2 [33, 34]. Moreover, because of the position of the valence band edge of both NiO and ZnO oxides (+ 2.34 eV for NiO and + 2.99 eV for ZnO), there is potential to oxidize the dye to carbon dioxide and water with NiO and ZnO by the aforementioned holes [31, 32]. The position values of the two semiconductors in zero charge point are calculated using the following relationships [27].

$$E_{BV} = X - E_e + 0.5E_g \quad (4)$$

$$E_{BC} = E_{BV} - E_g \quad (5)$$

where E_{VB} is the potential of the valence band edge, and ECB is the potential of the conduction band edge, X is the electro-negativity value ($X_{NiO} = 5.75$ eV, $X_{ZnO} = 5.79$ eV, $X_{MnO2} = 5.315$ eV), E_e is the energy of free electrons at the level of hydrogen (~ 4.5 eV) and Eg is the band width of the semiconductor. The coexistence of the three oxides, NiO, MnO_2, and ZnO, increase the rate of •OH in a very remarkable manner, compared to the case of only NiO. The formation of the holes is based on the chemical nature of NiO, ZnO, and MnO_2. This may explain the high rate of orange II degradation in samples based on three oxides compared to other cases.

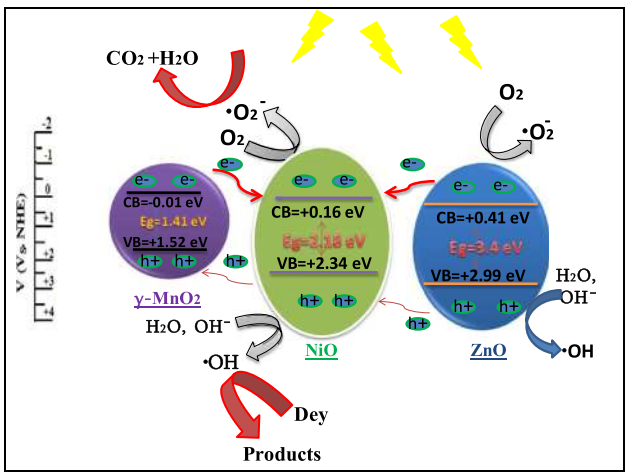

Fig. 9 The photocatalytic composite mechanism NiO/γ-MnO_2/ ZnO under visible light

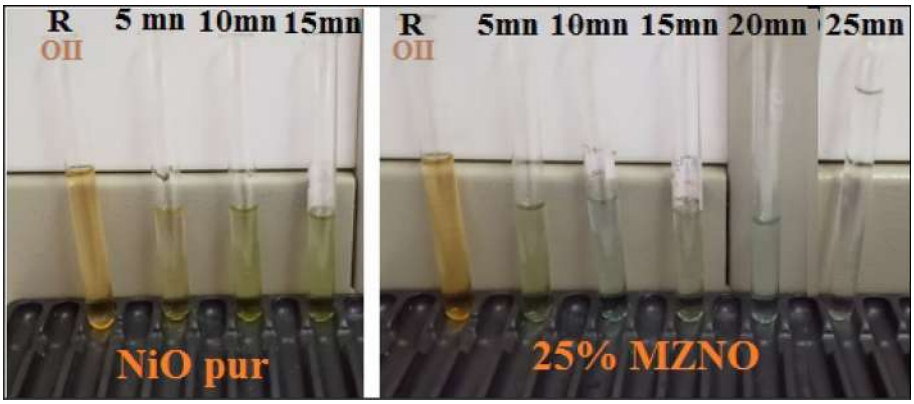

Fig. 10 Image showing the discoloration of OII for different durations of exposure under visible light

Upon completion of the phase of getting rid of the dangerous organic compounds resulting from the OII dye in the solution, the second phase begins, which is to remove the green color of the solution emitted from the used nickel oxide, through all the $\bullet O_2^-$ radicals of MZNO that contribute to giving the solution white (Fig. 10). Thus, a complete mineralization of the molecules present in the solution forms H_2O and CO_2 (Eq. 10) [26, 35]. Here are the chemical equations:

$$\begin{aligned} &NiO + ZnO + MnO_2 + hu_{\wedge} \\ &NiO\,(e^-) + NiO\,(h^+) + ZnO\,(e^-) \\ &+ ZnO\,(h^+) + MnO_2(e^-) + MnO_2(h^+) \end{aligned} \quad (6)$$

$$NiO\,(e^-) + MnO_2(e^-) + ZnO\,(e^-) + O_2 + H_2O \rightarrow \bullet O + \bullet HO_2^- \quad (7)$$

$$NiO\,(h^+) + MnO_2(h^+) + ZnO\,(h^+) + OH^- + H_2O \rightarrow OH\bullet \quad (8)$$

$$OH\bullet + Dey \rightarrow \text{mineralization dye} \quad (9)$$

$$\bullet O_2^- + \bullet HO_2^- + \text{mineralization dye} \rightarrow CO_2 \uparrow + H_2O \quad (10)$$

5 Conclusion

A very positive result was obtained while using expired nickel oxide powder with different addition ratios of zinc and manganese elements in the photocatalysis process. MZNO nanocomposites were prepared by sol–gel technique. Its structural analysis shows the presence of deformation accompanied by a shift of the peaks, and the increase in the percentage of addition led to an increase in the size of the grains of the compound, which was estimated at 30.33 nm while it was 21.28 nm. Their morphological analysis by SEM proved that the nanocomposite has globule-like growth providing a wider active area. The IR spectrum enabled us to observe the prominence of the absorption peaks of NiO, ZnO, and γ-MnO_2. Greater absorption of the energy of visible light photons was associated with an increase in absorbance with doping. The final results showed that the ZMNO nanocomposite is effective as a catalyst to break down the organic dye orange II under visible light. The photocatalytic process went through stages to remove the final dye and obtain CO_2 and H_2O, where the total dissolution time was 25 min for the 25%MZNO sample.

Acknowledgements This work has been supported by the Laboratory of active components and materials University Larbi Ben Mhidi Oum El Bouaghi, Algeria.

Declarations

Conflict of interest The authors declare that they have unknown competing financial interests or personal relationships that could appeared to influence the work reported in this paper.

References

1. M. Humayun, C. Wang, W. Luo, Recent progress in the synthesis and applications of composite photocatalysts: a critical review. Small Methods. **6**(2), 2101395 (2021). https://doi.org/10.1002/smtd.202101395
2. D. Bouras, M. Rasheed, R. Barille, Mustafa Nuhad Aldaraji, Efficiency of adding DD3+(Li/Mg) composite to plants and their fibers during the process of filtering solutions of toxic organic dyes. Opt. Mater. **131**, 112725 (2022). https://doi.org/10.1016/j.optmat.2022.112725
3. X. Liu, W. Chen, C. Zhang, T. Li, J. Huang, G. Chen, T. Shao, T. Gong, K. Ostrikov, Heterostructured palladium-nickel sulfide on plasma-activated nickel foil for robust hydrogen evolution. Am Chem Soc. **10**(24), 8064–8074 (2022). https://doi.org/10.1021/acssuschemeng.2c02133
4. A.A. Ezhilarasi, J.J. Vijaya, K. Kaviyarasu, X. Zhang, L.J. Kennedy, Green synthesis of nickel oxide nanoparticles using Solanumtrilobatum extract for cytotoxicity, antibacterial and photocatalytic studies. Surf. Interfaces. **20**, 100553 (2020)

5. M. Qin, Y. Li, H. Zhang, M. Humayun, X. Xu, Y. Fu, M.K. Kadirov, C. Wang, Crystalline/amorphous heterostructure offering highly efficient overall water splitting and urea electrolysis. J. Alloy. Compd. **921**, 166071 (2022)
6. Q. Wang, K. Domen, Particulate photocatalysts for light-driven water splitting: Mechanisms, challenges, and design strategies. Chem. Rev. **120**, 919–985 (2020). https://doi.org/10.1021/acs.chemrev.9b00201
7. I.D. Farrukh, R.M. Kevin, E.S. Mohammed, Morphology and property control of NiO nanostructures for supercapacitorapplications. J. Nanoscale Res. Lett. **8**, 363 (2013)
8. V. Julijana, P.G. Margareta, N. Metodija, S. Nace, Studies on electrochromism of chemically deposited nickel oxide thin films. Silpakorn U. Sci. Tech J. **5**(1), 34–42 (2011)
9. J.S. Anandh, M. Haris, P. Immanuel, Structural and optical properties of pure nio and li-doped nickel oxide thin films by sol-gel spin coating method. Int. J. Sci. Res. **23**, 58–87 (2014)
10 J. Wang, J. Luo, D. Liu, S. Chen, T. Peng, One-pot solvothermal synthesis of MoS2-modified Mn0.2Cd0.8S/MnS heterojunction photocatalysts for highly efficient visible-light-driven H2 production. Appl. Catal. B-Environ. **160**(161), 614–620 (2014). https://doi.org/10.1016/j.apcatb.2018.09.033
11. Y. Jiao, Q. Huang, J. Wang, Z. He, Z. Li, A novel MoS_2 quantum dots (QDs) decorated Z-scheme g-C_3N_4 nanosheet/N-doped carbon dots heterostructure photocatalyst for photocatalytic hydrogen evolution. Appl. Catal. B-Environ. **247**, 124–132 (2019). https://doi.org/10.1016/j.apcatb.2019.01.073
12. H. Wang, G. Wu, X.P. Cai, Y. Zhao, Z.F. Shi, J. Wang, X.C. Xia, X. Dong, B.L. Zhang, Y. Ma, G.T. Du, Effect of growth temperature on structure and optical characters of NiO films fabricated by PA-MOCVD. Vacuum **86**, 2044–2047 (2012)
13. M. Yang, H. Pu, Q. Zhou, Q. Zhang, Transparent p-type conducting K-doped NiO films deposited by pulsed plasma deposition. Thin Solid Films **520**, 5884–5888 (2012)
14. A. Loukil, A. Boukhachem, M. BenAmor, M. Ghamnia, K. Raouadi, Effects of potassium incorporation on the structural, optical, vibrational and electrical properties of NiO sprayed thin films for p-type optical windows. Ceram. Int. **42**, 8274–8289 (2016)
15. M. Das, K.G. Bhattacharyya, Oxidation of rhodamine B inaqueous medium in ambient conditions with raw and acidactivated MnO_2, NiO, ZnO as catalysts. J Mol. Catal. A Chem. **391**, 121–129 (2014)
16. Y.-L. Chan, S.-Y. Pung, S. Sreekantan, F.-Y. Yeoh, Photocatalytic activity of β-MnO_2 nanotubes grown on PET fibreunder visible light irradiation. J. Exp. Nanosci. **11**(8), 603–618 (2016)
17. A. Baral, D.P. Das, M. Minakshi, M.K. Ghosh, D.K. Padhi, Probing environmental remediation of RhB organic dye using α-MnO_2 under visible-light irradiation: structural, photocatalytic andmineralization studies. Chem Select. **1**(14), 4277–4285 (2016)
18. Z. Ai, L. Zhang, F. Kong, H. Liu, W. Xing, J. Qiu, Microwave assisted green synthesis of MnO_2 nanoplates with environmental catalytic activity. Mater Chem. Phys. **111**(1), 162–167 (2008)
19 Y.L. Chan, S.Y. Pung, N.S. Hussain, S. Sreekantan, F.Y. Yeoh, Photocatalytic degradation of rhodamine B using MnO_2 and ZnO nanoparticles. Mater Sci Forum. **756**, 167–174 (2013)
20. J.-H. Cheng, G. Shao, H.-J. Yu, J.-J. Xu, Excellent catalytic and electrochemical properties of the mesoporous MnO_2 nanospheres/nanosheets. J Alloys Compd. **505**(1), 163–167 (2010)
21. K. Saravanakumar, V. Muthuraj, S. Vadivel, Constructing novel Ag nanoparticles anchored on MnO_2 nanowires as an efficient-visible light driven photocatalyst. RSC Adv **6**(66), 61357–61366 (2016)
22. D. Bouras, A. Mecif, R. Barillé, A. Harabi, M. Rasheed, A. Mahdjoub, M. Zaabat, Cu:ZnO deposited on porous ceramic substrates by a simple thermal method for photocatalytic application. Ceram. Int. **44**, 21546–21555 (2018)
23. D. Bouras, A. Mecif, R. Barillé, A. Harabi, M. Zaabat, Porosity properties of porous ceramic substrates added with zinc and magnesium material. Ceram. Int. **46**, 20838–20846 (2020)
24. A. Rahda, M. Aliahmad, Y. Azizi, NiO Nanoparticles: synthesis and characterization. JNS. **5**, 145–151 (2015)
25. S.A. Jesuraj, M. Haris, P. Immanuel, Immanuel structural and optical properties of pure NiO and Li-doped nickel oxide thin films by sol-gel spin coating method. Int. J. Sci. Res. **23**, 58–87 (2014)
26. D. Bouras, A. Mecif, A. Harabi, R. Barillé, A.H. Mahdjoub, M. Zaabat, Economic and ultrafast photocatalytic degradation of orange II using ceramic powders. Catalysts **11**, 733 (2021)
27. F. Moulai, O. Fellahi, B. Messaoudi, T. Hadjersi, L. Zerroual, Electrodeposition of nanostructured γ-MnO2 film for photodegradation of Rhodamine B. Electron. Suppl. Mater. (2018). https://doi.org/10.1007/s11581-018-2440-7
28 V. Sannasi, K. Puchamy, Influence of Moringaoleifera gum on two polymorphs synthesis of MnO_2 and evaluation of the pseudocapacitance activity. J. Mater. Sci. Mater. Electron. (2020). https://doi.org/10.1007/s10854-020-04272-z
29 N.A. Khan, K. Saeed, I. Khan, T. Gul, M. Sadiq, A. Uddin, I. Zekker, Efficient photo degradation of orange II dye by nickel oxide nanoparticles and nanoclay supported nickel oxide nanocomposite. Appl. Water Sci. (2022). https://doi.org/10.1007/s13201-022-01647-x
30 X. Zhang, J. Ma, C. Fan, S. Komarneni, Enhancement of photo-fenton-like degradation of orange II by MnO_2/NiO nanocomposite with the synergistic effect from bisulfate. J. Alloys Comp. (2019). https://doi.org/10.1016/j.jallcom.2019.01.197
31. J. Wen, X. Li, W. Liu, Y. Fang, J. Xie, Y. Xu, Strategies for engineering metal-organic frameworks as efficient photocatalysts. Chin. J. Catal. **36**, 2049–2070 (2015). https://doi.org/10.1016/S1872-2067(15)60999-8
32. S. Zhao, J. Xu, Z.T. Li, Z.Y. Liu, Y.R. Li, Molybdenum disulfide coated nickel-cobalt sulfide with nickel phosphide loading to build hollow core-shell structure for highly efficient photocatalytic hydrogen evolution. J. Colloid. Interf. Sci. **555**, 689–701 (2019). https://doi.org/10.1016/j.jcis.2019.08.019
33. M.M. Najafpour, A.N. Moghaddam, H. Dau, I. Zaharieva, Fragments of Layered Manganese Oxide Are the Real Water Oxidation Catalyst after Transformation of Molecular Precursor on Clay. J. Am. Chem. Soc. **136**, 7245–7248 (2014)
34. I. Khan, M. Luo, S. Khan, H. Asghar, M. Saeed, S. Khan, A. Khan, M. Humayun, L. Guo, B. Shi, Green synthesis of SrO bridged $LaFeO_3$/g-C_3N_4 nanocomposites for CO_2 conversion and bisphenol A degradation with new insights into mechanism. Environ. Res. **7**, 112650 (2022). https://doi.org/10.1016/j.envres.2021.112650
35. M. Wiechen, M.M. Najafpour, S.I. Allakhverdiev, L. Spiccia, Water oxidation catalysis by manganese oxides: learning from evolution. Energy Environ. Sci. **7**, 2203–2212 (2014)

Publisher's Note Springer Nature remains neutral with regard to jurisdictional claims in published maps and institutional affiliations.

Springer Nature or its licensor holds exclusive rights to this article under a publishing agreement with the author(s) or other rightsholder(s); author self-archiving of the accepted manuscript version of this article is solely governed by the terms of such publishing agreement and applicable law.